Faraday Discussions

Accepted Manuscript

This manuscript will be presented and discussed at a forthcoming Faraday Discussion meeting. All delegates can contribute to the discussion which will be included in the final volume.

Register now to attend! Full details of all upcoming meetings: http://rsc.li/fd-upcoming-meetings

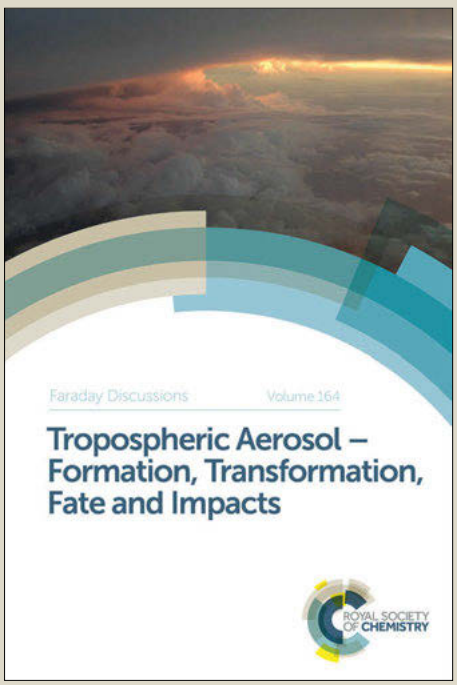

This is an *Accepted Manuscript*, which has been through the Royal Society of Chemistry peer review process and has been accepted for publication.

Accepted Manuscripts are published online shortly after acceptance, before technical editing, formatting and proof reading. Using this free service, authors can make their results available to the community, in citable form, before we publish the edited article. We will replace this *Accepted Manuscript* with the edited and formatted *Advance Article* as soon as it is available.

You can find more information about *Accepted Manuscripts* in the Information for Authors.

Please note that technical editing may introduce minor changes to the text and/or graphics, which may alter content. The journal's standard Terms & Conditions and the Ethical guidelines still apply. In no event shall the Royal Society of Chemistry be held responsible for any errors or omissions in this *Accepted Manuscript* or any consequences arising from the use of any information it contains.

ROYAL SOCIETY OF CHEMISTRY

www.rsc.org/faraday_d

Multi-colour pulses from seeded free-electron-lasers: towards the development of non-linear core-level coherent spectroscopies.

Filippo Bencivenga[a], Flavio Capotondi, Francesco Casolari, Francesco Dallari, Miltcho B. Danailov, Daniele Fausti, Maya Kiskinova, Michele Manfredda, Claudio Masciovecchio[b] and Emanuele Pedersoli

DOI: 10.1039/b000000x [DO NOT ALTER/DELETE THIS TEXT]

We report on new opportunities for ultrafast science thanks to the use of two-colour extreme ultraviolet (XUV) pulses at the FERMI free electron laser (FEL) facility. The two pulses have been employed to carry out a pioneering FEL-pump/FEL-probe diffraction experiment using a Ti target and tuning the FEL pulses to the $M_{2/3}$-edge in order to explore the dependence of the dielectric constant on the excitation fluence. The future impact that the use of such a two-colour FEL emission will have on the development of ultrafast wave-mixing methods in the XUV/soft x-ray range is addressed and discussed.

PACS: 41.60.Cr 78.47.jh 78.47.J-

1 Introduction

The last decades have witnessed the advent of two new classes of photon sources: optical lasers and synchrotrons, that are presently used in several fields of physics, chemistry and biology. Synchrotrons can provide high brightness photon pulses of 10-100 ps time duration ranging from the extreme ultraviolet (XUV) to the hard x-rays. A distinct feature of synchrotrons is the broad emission spectrum, that permits to achieve continuous tunability in the photon energy while retaining a sufficient photon flux at the sample. This has allowed the development of core-level spectroscopies, e.g.: x-ray absorption and emission, anomalous diffraction, resonant inelastic x-ray scattering, etc. In all these methods, the source tunability across core transitions of selected elements permits to obtain information on the electronic, molecular and lattice structures of the sample with element and chemical state sensitivity. On the other hand, the pulse duration hampers the study of ultrafast (< ps) processes. Only recently pioneering experiments succeeded in using synchrotrons to probe ultrafast dynamics induced by optical laser pulses ('pump').[1-3]

Optical lasers are able to provide coherent photon pulses as short as few fs with brightness larger than synchrotrons. Furthermore, the spatial and temporal coherence of laser radiation ensures the occurrence of fixed phase relationships between the values of the electric field in different positions and times. This feature is at the base of applications such as interferometry or holography and also allowed the prompt discovery of non-linear wave-mixing phenomena.[4] Methods based on optical wave-mixing[5,6,7] (e.g., transient grating,[8] photon echo,[9] coherent Raman scattering,[10] etc.)

can probe a large timescale range and can provide selectivity in the probed excitations. To date, these methods are exploited in several fields of physics, chemistry and biology to study a large array of dynamical processes, ranging from ms diffusions[11] and μs-ns protein folding[12] to sub-ps reconstruction of wavefunction in reacting molecules,[13] electronic relaxations and charge transfers.[9] The major limitation of these experiments is the long wavelength of optical radiation produced by table top lasers. This prevents the excitation of core-level transitions, that can be exploited to obtain atomic selectivity.

Such limitation can be overcome by XUV/x-ray wave-mixing methods, as already theoretically discussed in details.[14-17] As compared to (linear) pump-probe core-level spectroscopies, XUV/x-ray wave-mixing methods are potentially able to probe the non-local nature of the excitations as well as coherences between different atoms within a molecule,[14-17] thus potentially allowing to study, e.g., charge and energy transfer processes at the molecular scale with elemental sensitivity.

However, the requirements in terms of coherence, pulse duration and field intensity are beyond the capabilities of the most advanced synchrotron sources. On the other hand, sources based on the high-harmonic-generation process are able to deliver ultrafast coherent XUV/x-ray pulses[18] but, at the present stage of their development, cannot provide the required field intensity and have limited wavelength tunability. In this respect the advent of free electron laser (FEL) sources, providing ultrafast XUV/x-ray photon pulses with high field intensity, represents an opportunity for extending wave-mixing methods in the XUV/x-ray range. Recently, the FEL photons from LCLS (Stanford, USA) have been used to demonstrate a wave-mixing process involving x-ray photons, still with the assistance of an optical laser.[19] Furthermore, *"with an eye toward extending optical wave-mixing techniques to the x-ray regime"*,[20] the LCLS team recently demonstrated the first two-colour FEL emission, still in the self amplified spontaneous emission (SASE) regime. This is characterized by an emission spectrum consisting in several longitudinal modes with random phase relations among them, which results in a poor longitudinal (time) coherence. A two-colour SASE FEL emission has also been reported from SACLA facility (Koto, Japan).[21]

Highly coherent ("laser-like") FEL pulses can be obtained through a seeding process, which also reduces significantly the shot-to-shot fluctuations of the FEL output.[22] Seeding is adopted at LCLS (for the single-colour operation) and at FERMI (Elettra, Trieste, Italy). The scheme developed at FERMI is based on an ultrafast UV laser that triggers the FEL emission.[22] This makes possible to control the FEL output by tuning the seed laser. For instance, the FEL photon energy is given by $\hbar\omega_{FEL}=N\hbar\omega_{UV}$, where $\hbar\omega_{UV}$ and N are the photon energy of the seeding pulse (tunable in the 4-5.5 eV range[‡]) and an integer (harmonic) number, respectively. The latter is presently limited to the 3-15 range, but in a near future N values up to 60-70 will be possible by exploiting a double stage FEL scheme.[23] The possibility to chose both $\hbar\omega_{UV}$ and N allows for a continuous tunability in $\hbar\omega_{FEL}$.[24] In summary, seeded FELs, as FERMI, combine the key advantages of synchrotron and laser sources. Furthermore, we recently demonstrated the possibility to achieve a two-colour (easily upgradable at 'multi-colour') seeded FEL emission with independent control on relative intensity, time delay (Δt) and photon energy separation ($\Delta\omega$) between the two FEL pulses.[25]

Such a two-colour FEL emission has been employed to study the XUV optical response of Ti 0.5 ps after the FEL irradiation.[25] The obtained results suggest the

occurrence of a FEL-induced XUV transparency for fluences (F) larger than 2 J/cm^2, which can be qualitatively accounted for by a frequency shift (> 2.2 eV) of the optical constants of the Ti sample. However, the limited set of data did not allowed us to quantify the amount of the shift nor to study its dependence on F. The latter is often the key variable for this class of experiments, since it ultimately determines the amount of energy transfer to the sample. In order to fill this gap of knoweledge, we hereby report the results of new two-colour FEL-pump/FEL-probe measurements on Ti as a function of F.

In the F-range exploited in the present study a tangible photoionization occurs within the FEL pulse duration (~ 50 fs). This brings the system is into a non-equilibrium state consisting in a hot dense electron plasma and a cold ionic lattice. Such an "exotic" state evolves in the sub-ps timescale towards a thermodynamic equilibrium state, termed warm dense matter (WDM), that survives until the hydrodynamic expansion (typically after a few 10's of ps) ineluctably destroys the sample. The transient nature of WDM samples imposes experimental approaches based on ultrafast methods, even for the determination of basic quantities such as, e.g., temperature and density.[26,27,28,29,30] WDM is featured by extreme conditions of these thermodynamic parameters,[31] typical in astrophysical context.[32] The theoretical description of these extreme states of matter is a *grand challenge* for fundamental science. Indeed, on one hand, WDM is "too hot" to be described by classical condensed matter theories and, on the other hand, it is 'too dense' to be described in the frame of classical plasma. In these conditions the thermal energy compares to the Fermi energy and to the interaction energy of ions. This turns into a partial degeneracy of free electrons, strong couplings between ions and a significant population of excited states. These conditions lead to correlations between particles in the plasma and to the persistence of a short-range order. The understanding of these general aspects of interparticle interactions in solid density plasma is expected to have a deep impact, e.g., in the development of inertial confinement fusion technology.[33]

Since XUV/x-ray FELs can overcome the issue of the optical opacity of the induced electron plasma, they have already been exploited to study solid density plasma.[31] The unique capability to probe core electron states have enabled the discovery of new phenomena, as the saturation of core transitions at the L-edge of Al.[34] Such a pioneering experiment, carried out without time resolution, reveals how the inner-shell absorbers can be severely depleted when the photoionization rate surpasses the recombination one. This turns into a reduced screening of the electrostatic atomic potential, which shifts the absorption edge towards higher energy.[34-37] The lack of time resolution limits this kind of study to the non-equilibrium state reached within the time duration of the FEL pulse (i.e., ~ 15 fs for the experiment discussed in Ref. 34). An FEL-pump/FEL-probe approach is thus required to obtain direct information on the time evolution of the system towards the WDM regime. The changes in the diffraction pattern from grating-shaped samples irradiated with two-colour FEL pulses allowed us to determine the F-dependence of both the absorption (β) and dispersion coefficients (δ) of Ti at the expected time (~ 0.5 ps) for the transition towards the WDM state. With respect to absorption measurements,[34] in which only β can be determined, the present approach allows to obtain both δ and β and, therefore, to determine the F-dependence of the dielectric constant (ε). The latter quantity embodies relevant information on the electronic properties of the sample, that can be used, e.g., to map fast phase transitions induced

by FEL radiation,[38,39] such as interatomic bond softening.

The present study reports on the first determination of ε close to a core atomic resonance in FEL-excited matter undergoing a transition towards the WDM regime.

After the description of the two-colour FEL scheme developed at FERMI in Section II and the discussion of the results obtained from Ti in Section III, Section IV is dedicated on discussing the use of such a two-colour coherent emission in wave-mixing applications, that will be developed at FERMI in the near future.

2 Double seed pulse operation at FERMI

The basic idea to achieve a multi-pulse FEL emission at FERMI is very simple and consists in seeding the electron bunch with multiple seed laser pulses.[40] Fig. 1a shows the the two seed pulses obtained by splitting the incoming pulse from a Ti:sapphire laser (photon energy 1.58 eV, time duration 120 fs) in two pulses travelling through separate arms. One of them can be time delayed by a pair of insertable wedgess; the actual time delay is monitored by optical cross-correlation. Each beam path is equipped with independent filters, shutters and crystals for third harmonic generation, the latter being able to provide independent tunability in the photon energy of both pulses ($\omega_{UV,1}$ and $\omega_{UV,2}$) in the 4.77-4.73 eV range. A much wider range can be achieved by using an ultrafast UV optical parametric amplifier, also available at FERMI. The two UV seed pulses are finally collinearly recombined and sent into the FEL amplifier (main panel of Figure 1). As long as $\omega_{UV,1}$ and $\omega_{UV,2}$ are within the gain bandwidth of the FEL amplifier (of about 0.5-1 %), these seed pulses stimulate the two-colour FEL emission at $\omega_{FEL,1}=N\omega_{UV,1}$ and $\omega_{FEL,2}=N\omega_{UV,2}$.

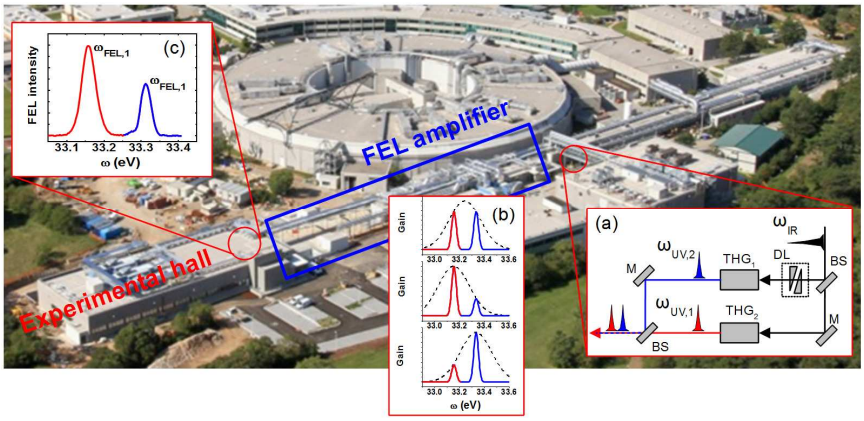

Fig. 1: (main panel) FERMI facility; the blu hatched area is the FEL amplifier. (a) Optical system used to obtain the two seed laser pulses: BS, M, $THG_{1,2}$ and DL are 50:50 beamsplitters, reflective mirrors, third harmonic generation crystals and the delay line, respectively. (b) Changes in the relative intensity between the two-colour FEL pulses as a function of the central frequency of the FEL gain curve (dashed lines); the blu/red double peak structure sketches the spectrum of the FEL output. (c) Spectrum of the FEL output measured during the experiment on Ti; $\omega_{FEL,1}$=33.16 eV and $\omega_{FEL,2}$=33.32 eV are the pump and probe pulses, respectively.

The relative intensity between the two FEL pulses can be varied either by acting on the pulse energy of the seeds or by shifting in ω the gain bandwidth of the FEL, as sketched in Fig. 1b. Each of the two FEL pulses can be blocked by simply closing the shutter in the corresponding seed laser beamline. The FEL output is monitored shot-by-shot by an "on-line" XUV/soft x-ray spectrometer.[41] A representative two-colour FEL spectrum is reported in Fig. 1c. The jitters in intensity and photon energy were of about 15 % and 0.005 %, respectively, while $\delta\omega/\omega_{FEL} \sim 5*10^{-4}$, where δω is the FEL pulse bandwidth. Such a very narrow (almost transform limited) bandwidth and the extremely low jitters are the practical manifestations of the "laser-like" features of the seeded FEL emission. The two-colour pulses are also expected to be coherent (i.e., to have fixed phase relationship among them), since they arose from the same (coherent) laser pulse and the scheme adopted at FERMI allows to preserve the coherence properties of the seed laser in the FEL emission.[42] The time jitter between the two pulses is expected to be negligible (< 1 fs), since it may only be due to fluctuations in the optical path difference accumulated by the two pulses along the beam paths shown in Fig. 1a, where they are separated. These paths are quite short (~ 0.5 m) and are situated in stable environmental conditions. In support of this statement we refer to recent timing measurements, where we found that jitters introduced by a very complex and ~150 m long beam transport of the seed laser down to the FERMI experimental hall are in the sub-10 fs range.[43]

The maximum separation in $\Delta\omega=\omega_{FEL,1}-\omega_{FEL,2}$ is presently limited to $\sim 0.01*\omega_{FEL}$ by the bandwidth of the FEL amplifier; larger Δω-values can be obtained at the expense of the intensity. Strategies to extend the exploitable Δω-range up to a few % of ω_{FEL} are under evaluation. The Δt range is also limited to values shorter than the length of the electron bunch (~1 ps), while interference effects occurring when the two seed pulses overlap in time set the lower limit for Δt at about 0.2-0.3 ps. The latter can be reduced by exploiting seed laser pulses shorter than the ones used here. Alternatively, a single chirped seed pulse with very high intensity can be used to achieve a two-colour FEL emission with Δt-values in the sub-100 fs range[44] or, eventually, exploiting seeding schemes with light pulses with ortogonal polarization (both 45° with respect to the axis of the modulator).

3 Absorptionless and dispersiveless behaviour of Ti in the sub-ps timescale induced by FEL-irradiation

Measurements have been carried out at the DiProI experimental end-station.[45,46] The value of Δt was set to 0.5 ps, a value much shorter than the characteristic timescale for hydrodynamic expansion. The photon energy of the pump pulse ($\omega_{FEL,1}$) was set to 33.16 eV, i.e. across the Ti $M_{2,3}$-edge, while the photon energy of the probe one ($\omega_{FEL,2}$) was set to 33.32 eV, still within the Ti $M_{2,3}$-edge slope. The collinearity of the two FEL pulses hitting the target was checked by means of in-situ and ex-situ methods, that also allowed to estimate the focal spot area (~ 1000 μm^2) provided by a Kirkpatrick–Baez active optical system.[47,‡‡] The total FEL intensity was measured shot-by-shot by two I0 monitors placed after and before a gas attenuator cell.[41] The latter was used in combination with solid state filters to modify the intensity of the FEL pulses. The residual UV radiation from the seed laser was blocked by an Al filter. The area of each spectral line (see Figure 1c) can also be used as a measure of the FEL pulse intensity, both in single or double pulse mode.

This parameter showed a good correlation with both the I0 monitor and a thermopile sensor, placed in the experimental end-station before the experiment for calibration purposes. The maximum FEL intensity at the sample was ~10 μJ, corresponding to a maximum F-value of ~1 J/cm^2; the damage threshold of the sample was found to be ~ 0.1 J/cm^2. The estimated time duration of the FEL pulses was 75 fs.[48,49]

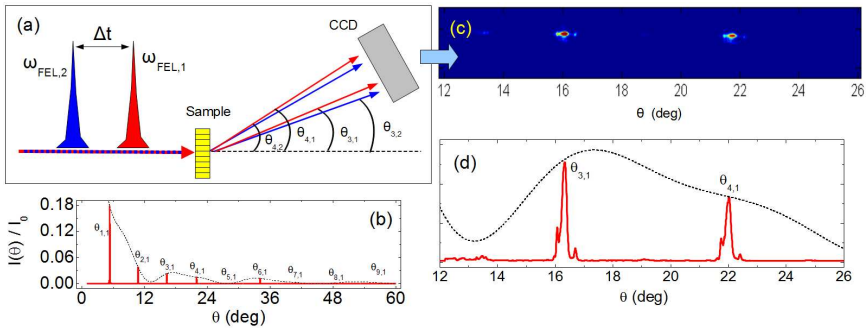

Fig. 2: (a) Sketch of the experimental setup: $\theta_{3,1}$, $\theta_{3,2}$, $\theta_{4,1}$ and $\theta_{4,2}$ are the diffraction angles (enlarged for clarity) collected by the CCD detector, Δt=0.5 ps is the pump-probe delay while $\omega_{FEL,1}$=33.16 eV and $\omega_{FEL,2}$=33.32 eV are the FEL photon frequencies. (b) Full red and dashed black lines are the expected lineshape of $I(\theta)/I_0$ at $\omega_{FEL,1}$ and the modulating function $F(\theta,\delta,\beta)$, respectively. The angular positions ($\theta_{N,1}$) of the first nine diffraction spots (N=1-9) are indicated. (c) Diffraction pattern from the Ti grating illuminated by a single FEL pulse at $\omega_{FEL,1}$, the bright spots located at $\theta\approx16.4^o$ and $\theta\approx22^o$ are the third and fourth order diffraction spots, respectively. (d) Full red and dashed black lines are the projected lineshape along θ of the image shown in panel (c) and the $F(\theta,\delta,\beta)$ profile scaled by an arbitrary factor, respectively.

The samples were gratings of 400 nm pitch (L) made out of parallel rectangular Ti bars (50 μm long, 165 nm wide and 70 nm thick) deposited on a 20 nm thick Si_3N_4 window; the total area of each sample was 50x50 μm^2. Since at the highest F-values the sample is destroyed by a single FEL shot, a matrix consisting in 169 (nominally identical) samples is used. The FEL pulses impinge onto the sample at normal incidence (see Fig. 2a). The intensity distribution of the diffracted intensity is reported in Fig. 2b, as calculated from the Huygens-Fresnel principle in the far field approximation, which is appropriate in the present case. Such a lineshape is given by $I(\theta)/I_0=R(\theta)F(\theta)$, where I_0 is the intensity of incident radiation while $R(\theta)$ and $F(\theta,\delta,\beta)$ are, respectively, the N-slits interference pattern and a modulating function that depends on δ, β and sample geometry (dashed line in Fig. 2b). $R(\theta)$ is featured by a set of peaks located in correspondence of given directions, defined by the angles $\theta_{N,i}=\sin^{-1}(2\pi Nc/\omega_{FEL,i}L)$ with respect the incoming beam direction in the plane ortogonal to the grating lines; here N is an integer number (diffraction order) while c is the speed of light. The grating sample thus works as a spectral analyser, since it is able to separate in angle the signal from the $\omega_{FEL,1}$ (pump) and $\omega_{FEL,2}$ (probe) radiation. However, since $L > 2\pi c/\omega_{FEL,i}$ while $\omega_{FEL,1} \approx \omega_{FEL,2}$, the angular separation between the $\omega_{FEL,1}$ and $\omega_{FEL,2}$ radiation diffracted in the same Nth order ($\delta\theta_N=\theta_{N,1}-\theta_{N,2}$) is much smaller than the angular separation between adiacent orders

($\theta_{N,i}$-$\theta_{N+1,i}$). $\delta\theta_N$ actually compares to the observed intrinsic angular spread of the diffraction peaks, which is mainly due to the finite number of illuminated lines of the grating and to the divergence (~ 0.2°) of the incoming (focused) beams. The lineshape of the N^{th} diffraction spot from the two-colour beam thus consists in a broadening of the peak with respect to the single colour diffraction spot, rather than in two well defined peaks. This situation makes more difficult to separately determine the amount of pump and probe signals, thus complicating the data analysis and interpretation. Such an undesired angular overlap between the pump and probe diffraction spots is mitigated at large N-values, since $\delta\theta_N$ increases on increasing N. For this reason we placed the CCD detector (Princeton Instrument MTE-2048B) to monitor the highest diffraction orders (i.e., N=3 and N=4; located in the 12°-26° θ-range), compatibly with the geometrical constraints of the experimental setup. An example of the measured diffraction pattern is shown in Fig. 2c, while in Fig. 2d we report the corresponding projected lineshape along the θ-axis. In this case $\delta\theta_N$ ~ 0.2° while the angular separation between the third and fourth diffraction orders is ~ 5°.

In the low-F regime (<< 0.1 mJ/cm^2), where the samples are not damaged by the FEL irradiation, three set of measurements were carried out: (i) only with the pump pulse, (ii) only with the probe one and (iii) with both pulses. These measurements consist in the acquisition of at least 100 FEL shots. After that, we performed a single-shot measurement with both pulses in the high-F regime (> 0.1 mJ/cm^2). Figs. 3a, 3b and 3c report the images of the fourth diffraction order for cases (i), (ii) and (iii), respectively, while Fig. 3d is the corresponding high-F pump-probe single-shot measurement. By inspecting these raw data one can appreciate how the diffraction spot of the low-F pump-probe measurement (Fig. 3c) is reasonably similar to the sum of the low-F signal from pump (Fig. 3a) and probe pulses (Fig. 3b), while the profile of the high-F pump-probe measurement (Fig. 3d) resembles that of the pump pulse alone (Fig. 3a). This qualitative observation can be quantified by extracting the projected lineshape along θ, which is shown in the right hand side of the respective images (Figs. 3e-3h). Fig. 3g shows how the diffraction lineshape of the low-F pump-probe measurements (blue circles) can be accounted for by a weighed sum of pump and probe profiles (solid red line), in which the weighting coefficients (C_{pump} and C_{probe}) are given by the intensity of pump and probe pulses, determined shot-by-shot by the 'on-line' spectrometer. This is not the case for the pump-probe lineshape at high-F (blue circles in Figs. 3h-3i). Here a decrease in the scattering intensity in the probe's side with respect to the expected weighted sum (magenta lines in Figs. 3h-3i) can be appreciated.

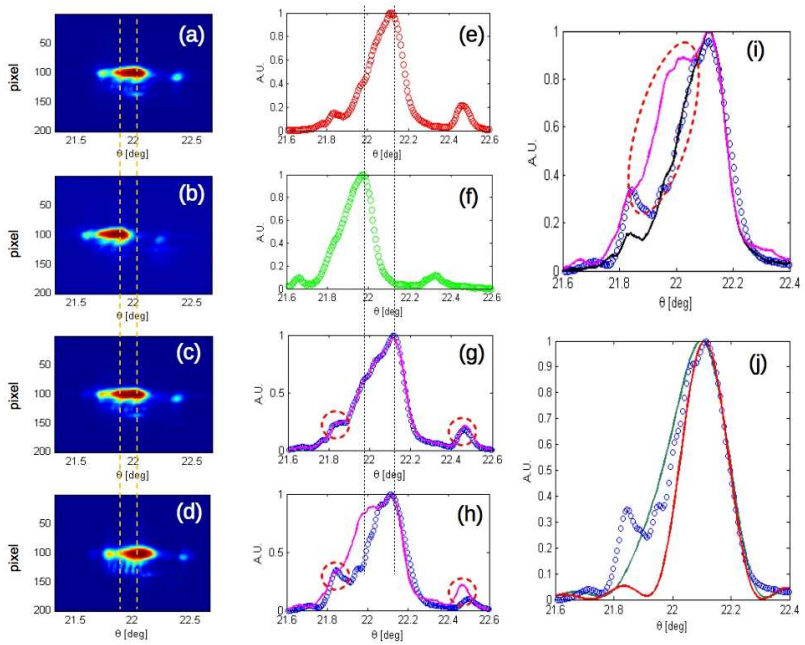

Fig. 3: panels (a) and (b) are, respectively, images of the fourth diffraction spot of the pump and probe pulses in the low-F regime (F<0.01 J/cm^2). Panels (c) and (d) are pump-probe profiles in the low-F (F<0.01 J/cm^2) and high-F (F=0.85 J/cm^2) regime, respectively. Data are scaled to the peak intensity; the vertical dashed lines mark the barycenter of pump and probe peaks. Dots in panels (e)-(h) are the projected lineshape along θ of the images in panels (a)-(d); pump, probe and pump-probe data are reported as red, green and blue dots, respectively, while magenta lines in panels (g) and (h) are the expected pump-probe lineshape; see text for further details. Dashed circles and vertical dashed lines in panels (g) and (h) indicate the satellite peaks and the barycenter of pump and probe peaks, respectively. Panel (i) compares the pump-probe lineshape at high-F (blue dots; F=0.85 J/cm^2) with the expected one (magenta line); the dashed ellipse highlights the decrease in the diffraction intensity in the probe's side. Black line is the result of the best fit procedure used to extract C_{pump}^{HF} and C_{probe}^{HF}; see text for further detail. Panel (j) compares the high-F pump-probe lineshape (blue dots) with the "starting" (green line) and "target" (red line) profiles used in the fitting procedure to determine δ and β at the probe's photon energy; see text for further details.

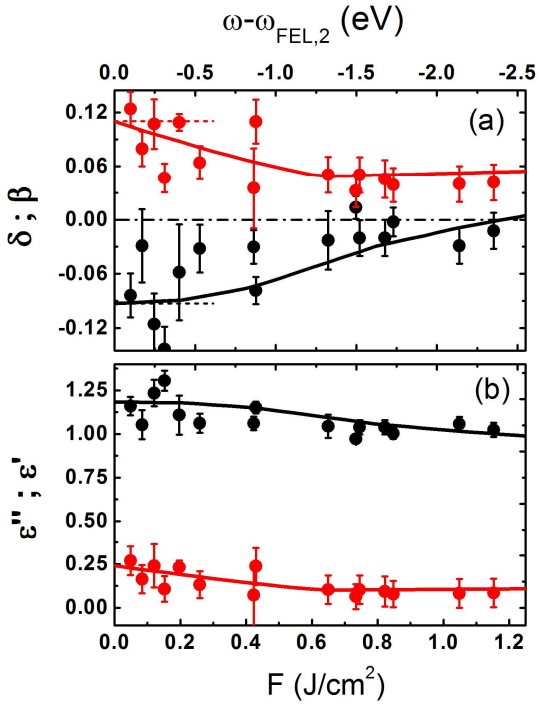

Fig. 4: (a) black and red dots are the experimental values of δ and β, respectively, as obtained through the fitting process outlined in the text. Dashed black and red horizontal lines indicate, respectively, the expected δ and β values for an unexcited Ti sample;[50] dash-dotted line corresponds to δ=β=0. Full black and red lines are the ω dependence (upper horizontal scale) of δ and β, respectively, as obtained from Ref. 42. (b) Corresponding F-dependence (bottom horizontal scale) of ε' (black dots) and ε'' (red dots); lines are the ω dependence of ε' and ε'' (upper horizontal scale).

Such a decrease in the probe scattering at high-F is our pump-probe signal, which can be ascribed to an F-induced change in the β and δ coefficients of Ti at the photon frequency of the probe. In order to confirm this hypothesis and quantify the eventual F-dependencies of δ and β we carried out a data analysis based on Huygens-Fresnel calculations. Specifically, since the sample parameters and the values of δ and β at $\omega_{FEL,1}$ and $\omega_{FEL,2}$ are known (δ and β data are from Ref. 50), we used the Huygens-Fresnel principle to calculate the expected diffraction lineshapes at $\omega_{FEL,1}$ and $\omega_{FEL,2}$. These profiles are then weighted by the measured values of C_{pump} and C_{probe} to obtain the expected diffraction pattern if no changes are induced by the pump. Such a lineshape is used as "starting profile" for a best fit procedure based on a standard χ^2 minimization in which the values of δ and β for the probe pulse are left free to vary in the Huygens-Fresnel calculations in order to match a "target profile" (see Fig. 3j). The latter is also calculated from the Huygens-Fresnel principle using as weighting coefficients (C_{pump}^{HF} and C_{probe}^{HF}) those obtained from a best fit procedure of the high-F pump-probe lineshape to a weighted sum of the

low-F profiles of pump and probe signals (see Fig. 3i). The analysis also assumes that the FEL does not induce changes in the Si_3N_4 substrate, which is essentially transparent at the employed FEL photon frequencies. The need to use such "artificial" starting and target profiles instead of the experimental data is due to imperfections in the sample morphology, that randomly vary from sample to sample. The only feature systematically observed is a pair satellite peaks, of unknown origin, whose relative intensity seems to systematically increase with F (see Figs. 3g-3h). These peaks were not taken into account in the data analysis.

The best fit results for δ and β are reported in Fig. 4a as a function of F. The quite large scattering of the data is mainly due to the aforementioned variability in the sample morphology and can be likely reduced by increasing the statistics (i.e., the number of samples probed in single-shot mode), as we are planning to do. However, in spite of the poor accuracy in the determination of δ and β, at low-F both quantities are consistent with the expected values while, on increasing F, they show the clear tendency to vanish.

On general grounds, the latter behavior is quite striking since in the XUV range materials may behave as a dispersiveless (δ→0) and absorptionless (β→0) medium only when probed far from atomic resonances, while the experiment has been carried out at the $M_{2/3}$ edge. This result can be cast in the frame depicted in Ref. 34, where saturable absorption of the Al L-transition reflects in an abrupt increase in the XUV transmission at fixed photon frequency with increasing F (FEL-induced transparency i.e. β→0 at high-F). Saturable absorption of the M-transition in Ti induced by the pump is expected to induces a shift of the absorption edge towards higher energy, due to the depletion of inner-shell absorbers.[34-37] Therefore, the subsequent probe radiation is no longer in resonance with this core transition and its optical response is similar to the one of the unperturbed sample irradiated with lower energy (out of resonance) photons. This picture is consistent with the observed trend, as highlighted in Fig. 4a, where we show the ω-dependence of δ and β for an unperturbed Ti sample (from Ref. 50) along with their F-dependence at fixed photon frequency ($\omega_{FEL,2}$=33.32 eV), as determined by the best fit procedure. It is worth noting that the FEL-induced transparency in Al was observed at a much faster timescale (< 15 fs), lying within the FEL pulse duration.[34] In fact, the results shown in Fig. 4 represent the first quantitative evidence of the persistence of a highly excited state featured by "XUV-transparency" at time scales (~ 0.5 ps) exceeding significantly the time duration of FEL excitation pulse (~ 0.05 ps) and, most importantly, the core-hole recombination time (<0.01 ps)[51] as well. Within 0.5 ps the sample most likely undergoes a tangible relaxation of the electronic and ion sub-systems and may have reached (or be close to) an extreme thermodynamic equilibrium state, as WDM. Consequently, our results indicate that in these conditions the system still shows qualitative similarities with the "exotic" (non-equilibrium) state occurring at much faster timescales. In particular, it may be featured by a non negligible amount of ionized atoms, likely in dynamic equilibrium with a warm free electron gas. In order to understand such dynamics we plan to systematically study the Δt-dependence of such phenomenology, though in a time window presently limited to 0.3-1 ps, as well as to enlarger the F-range (1-2 orders of magnitude more in F can be exploited in terms of FEL pulse energy and smaller focal spot size).

We finally recall that the proposed approach has the advantage to allow for the determination of both δ and β, from which it is straightforward to compute the

dielectric function: $\varepsilon=\varepsilon_0(\varepsilon'+i\varepsilon'')=\varepsilon_0(1-\delta+i\beta)^2$, where ε_0 is the free space permittivity. Results are shown in Fig. 4b. These represent the first time-resolved determination of ε in highly FEL-excited matter in correspondence of a core atomic resonance. More generally, the possibility to determine the time and fluence dependence of ε would be of great relevance for several applications, not necessarily limited to the study of matter under extreme conditions, since ε basically embodies all relevant information on the electronic properties of the sample.

The above described experiment has been carried out on a permanent ("static") grating. In the following section we describe how such a two-colour seeded FEL emission could be used to perform XUV/soft x-ray wave-mixing experiments, that are essentially based on "dynamic" gratings induced by the interference between coherent pulses.

4 Wave-mixing experiments with two-colour seeded FEL pulses

The experiment discussed in the previous section exploits the time and photon energy separation between the two FEL pulses and it undoubtedly points out the robustness of the two-color seeded FEL emission developed at FERMI. However, it does not directly use the full coherence provided by the seeding scheme, which would be exploited in the near future in XUV/soft x-ray wave-mixing experiments. The wave-mixing process results from the combined action of two or more input fields ($E_i(t)$), that may have different frequencies (ω_i) and wavevectors (k_i). The non-linear response of materials to these interacting fields can be accounted for by expressing the sample polarization in powers of $E_i(t)$, i.e.:[5]

$$P(t)=\varepsilon_0[\Sigma_i \chi^{(0)}E_i(t)+\Sigma_{i,j} \chi^{(2)}E_i(t)E_j(t)+\Sigma_{i,j,k} \chi^{(3)}E_i(t)E_j(t)E_k(t)+...]=P^L(t)+P^{NL}(t) \quad (eq.1)$$

where $\chi^{(n)}$ are tensors of rank n+1 termed n^{th}-order susceptibilities. The non linear polarization ($P^{NL}(t) = \varepsilon_0 [\Sigma_{i,j} \chi^{(2)}E_i(t)E_j(t) + \Sigma_{i,j,k} \chi^{(3)}E_i(t)E_j(t)E_k(t) + ...]$) acts as a driving force in the wave equation.[5] A n^{th}-order non-linear process can then lead to the radiation of electric fields at frequencies $\omega_{(n+1)wm}=\omega_1\pm\omega_2\pm...\pm\omega_n$, that are not necessarily present in the input fields. Such a non-linear mechanism is also referred to as (n+1)-wave-mixing process. In this frame the coherence of the input fields plays a crucial role, as it defines the phase relationships of P(t) in different locations and times within the sample. The $\omega_{(n+1)wm}$ radiation can thus add in amplitude rather than in intensity along a well defined, "phase-matched", direction $k_{(n+1)wm}=k_1\pm k_2\pm...\pm k_n$.[52,53] This leads to an N^2 increase in the intensity of the wave-mixing signal (where N is the number of elementary emitters in the sample falling within the coherence volume of the interacting fields), rather than the N scaling typical of any linear process obeying the superposition principle. Coherence may then result in an enormous increase in the non-linear signal from condensed matter, which can even turns into a well defined coherent beam propagating after the sample. It is worth stressing how such a phase matching argument does not hold for isolated atoms/molecules, in this case the non-linear signal will be emitted in all directions. Furthermore, in extended samples with inversion symmetry all the elements of the $\chi^{(2)}$ tensor vanish. In many practical cases the lowest order non-linear term is hence the $\chi^{(3)}$ one, which is associated to the four-wave-mixing (FWM) process. This is probably the non-linear mechanism more thoroughly

exploited in non-linear optical spectroscopy in condensed matter. A particular FWM method, also referred to as coherent Raman scattering (CRS), is reported in Figs. 5a. In this case two coherent beams ((ω_1,k_1) and (ω_2,k_2)) are crossed into the sample in time coincident conditions. The interference between these two pulses originates a (transient) electromagnetic wave with spatial periodicity $L=2\pi/|k_1-k_2|$ and 'beatings' at $\omega_1+\omega_2$ and $\omega_1-\omega_2$. The latter can be used, e.g., to stimulate a given excitation having characteristic energy $\omega_{ex}=\omega_1-\omega_2$, as illustrated in Fig. 5b. If a third coherent beam (ω_3,k_3) is sent into the sample in phase matching conditions (see Fig. 5c), then the time evolution of the selected excitation can be tracked back by looking at the intensity of the FWM signal at frequency $\omega_s=\omega_1-\omega_2+\omega_3$, that propagates along the 'phase matched' direction $k_s=k_1-k_2+k_3$.

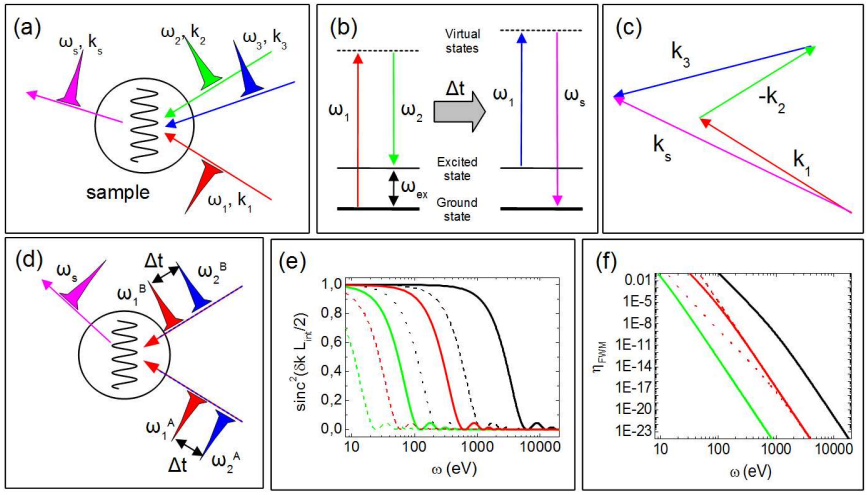

Fig. 5: Sketch of a FWM experiment: (b) input/output beams; (b) level scheme; (c) phase matching. (d) Sketch of a XUV CRS experiment that can be carried out at the EIS-TIMER beamline exploiting the two-colour operation of the FERMI FEL; note that the FWM signal (ω_s) propagates in a direction different from those of the input beams. (e) Phase matching factor for: $\delta k/k=1*10^{-4}$ and L_{int}=1, 10 and 50 μm (full, dashed and dotted black lines), $\delta k/k=1*10^{-3}$ and L_{int}=1 and 10 μm (full and dashed red lines), $\delta k/k=5*10^{-3}$ and L_{int}=1 and 10 μm (full and dashed green lines). (f) ω-dependence of η_{FWM} for resonant XUV/x-ray CRS (see text for further details) in the cases: $\gamma_0=0.01*\omega_0$, ω_{ex}=0.1, 1 and 10 eV (dashed, full and dotted red lines) and ω_{ex}=1 eV, $\gamma_0=0.001*\omega_0$, $0.01*\omega_0$ and $0.1*\omega_0$ (full black, red and green lines).

In optical CRS $\omega_{1,2,3}$ are limited to below ~3-4 eV, so that $\omega_1-\omega_2$ values are typically in the sub-eV range. This allows studying ultrafast dynamics of molecular vibrations and low-energy electronic excitations. In light of the larger field frequency of XUV/x-ray radiation, $\omega_1-\omega_2$ values as large as several eV's can be achieved. This would allow studying the ultrafast dynamics of high-energy ('optical') excitations, such as valence band excitons. In the XUV/x-ray range atomic selectivity of the FWM process can be also attained, since ω_1 and ω_3 can be tuned to core transitions of selected atoms in condensed samples. In this case the virtual states depicted in Fig. 5b are substituted by real core-hole resonances. The

localization of core shells ensures that the stimulated excitation is initially centered on the atom resonant at ω_1 (atom A), while the occurrence of a FWM signal at Δt means that the selected excitation propagated towards the atom resonant at ω_3 (atom B). The unique capability of XUV/x-ray FWM to stimulate high-energy excitations, as valence-band excitons, selecting the atomic specie in correspondence of which it is created as well as when and close to which atom it is eventually probed would allow, e.g., to study ultrafast charge transfers between different atomic species in molecular solids.[15,16,17,54,55]

The FWM process also provides wavevector selectivity through the k_s vector. For instance, in transient grating (TG) experiments $\omega_1=\omega_2$ and, consequently, only excitations with energy falling within the bandwidth of the excitation pulses can be stimulated. This is the case, e.g., of acoustic phonons, whose frequency continuously varies from zero to ~10-100 meV following a k-dispersion relation. Among all phonon modes that are excitable within the bandwidth of the excitation pulses, only the one with $k_s=k_1-k_2$ leads to a detectable (phase matched) FWM signal. The k_s-selectivity is of particular relevance in the XUV/x-ray range. Here the short wavelength of the radiation permits to probe k_s^{-1}-values that may compare with the characteristic lengthscales of inter- and intramolecular structures. The study of phonon modes in the so-called 'mesoscopic' k_s-range (0.1-1 nm^{-1}), nowadays inaccessible by any experimental method, is the main aim of the EIS-TIMER beamline.[56] The latter is a XUV/soft x-ray TG instrument that is going to be realized at FERMI in 2015 (a temporary setup with limited capabilities is ready to be hosted in the DiProI end-station for the first tests). Indeed, such a "mesoscopic" k_s-range is of the highest relevance for the study of collective atomic dynamics in disordered systems and nanostructures, since it matches the characteristic lengthscale of the topological disorder in the former class of samples and the "artificial" periodicity of the latter ones.

To date, the theoretical grounds for XUV/x-ray FWM methods have been already presented[14-17] and evidences of XUV wave-mixing are also available.[19,57,58] On such grounds we evaluated the possible impact of XUV/soft x-ray FWM, as well as the upgrades of the FERMI source and photon transport system to practically realize an 'ideal' XUV/soft x-ray FWM experiment, able to provide fs time resolution, polarization and atomic selectivity.[54,55]

In a short term perspective, the development of the two-colour seeded FEL emission opened up the way for additional wave-mixing applications (other than TG) at the EIS-TIMER end station. For instance, the photon transport system of EIS-TIMER will allow to split the FEL beam into two beamlines and then focus the two FEL beams at the sample with given crossing angles and variable time delays (up to some ps) among them.[56,59] This capability, in combination with the two-color operation, would permit, e.g., to realize the CRS experiment shown in Fig. 5d. In this case the first FEL pulse (ω_1^B) impinging into the sample is a "dummy pulse". Then two FEL pulses at ω_1 and ω_2 (labeled as ω_2^B and ω_1^A in Fig. 5d) are used to coherently stimulate excitations at $\omega_{ex}=\omega_1-\omega_2$, that are finally probed by the time delayed ω_2^A pulse. Atomic selectivity in the excitation process can be achieved by tuning ω_1 to a core transition of a given atom within the sample. In order to estimate the amount of the FWM signal expected in this kind of experiments (on condensed matter), we may considered the following equation:[54]

$$\eta_{FWM} = |E_s|^2 / |E_2^A|^2 = |\chi^{(3)}|^2 |E_1^A|^2 |E_2^B|^2 \exp^{-\alpha L} \mathrm{sinc}^2(\delta k L_{int}/2), \qquad (eq.2)$$

where η_{FWM} is the efficiency of the FWM process, E_s and E_2^A are the signal and probe fields, respectively, while the $\exp^{-\alpha L}$ factor accounts for the signal loss due to absorption, being L and α the length of the sample crosses by the probe beam and the absorption coefficient at the probe's frequency, respectively. Finally, the $\mathrm{sinc}^2(\delta k L_{int}/2)$ term in Eq. 2 is the phase matching factor, where L_{int} is the characteristic dimension of the overlapping volume of the input fields and δk is the wavevector mismatch. The latter defines the coherence length of the FWM process ($L_{FWM}=\pi/\delta k$). When $L_{FWM} > L_{int}$ the whole portion of the sample illuminated by the input beams gives rise to the FWM signal. Conversely, if $L_{FWM} < L_{int}$, then only an effective fraction of the interaction region coherently contributes to the FWM process. This situation may reflect in a substantial decrease of the signal; we recall that detectable XUV/x-ray FWM signals are expected from condensed samples owing to the coherent addition of scattering amplitudes occurring along the phase matching direction. In a non-collinear geometry δk is determined by both the pointing and wavelength stability of the source. The impact of the latter in a two-color wave-mixing experiment with $\omega_1 \sim \omega_2 = \omega$ and $\delta k_1 \sim \delta k_2$ is quantified in Fig. 5e, where we report the ω-dependence of the phase matching factor for some values of L_{int} and δk/k. In light of the excellent wavelength stability provided by seeding ($\delta k/k < 10^{-4}$)[22], a quite large value of L_{int} (of about 10 μm, compatible with the focal spot size routinely achieved at FERMI) can be attained. This is enough to keep the phase matching factor above an acceptable level throughout the entire ω-range (12-310 eV) exploitable by FERMI. On the other hand, the phase matching constraint becomes stricter on going deeper into the x-ray domain. Indeed, a given wavelength stability of the source (say $\delta k/k \sim 10^{-4}$) corresponds to much smaller L_{int}-values (~ 1 μm). Smaller focal spot sizes are hence necessary to keep the phase matching factor at the same level (see Fig. 5e). An estimate of the magnitude of $|\chi^{(3)}|$ can be gained by the following equation:[5]

$$\chi^{(3)}=(3ne^4\omega_0^2)/[8\varepsilon_0 m_e^3 r_a^2|\omega_1^2-\omega_0^2-2i\gamma_0\omega_1|^2(\omega_2^2-\omega_0^2-2i\gamma_0\omega_1)^2], \qquad (eq.3)$$

where n, r_a, e and m_e are the number density, the atomic radius, the electron charge and mass, respectively, while ω_0 and γ_0 are the characteristic energy and linewidth of the involved core transition. Fig. 5f reports the corresponding ω_1-dependence of η_{FWM} for different values of ω_{ex} and γ_0, as obtained from Eqs. 2-3 by assuming that one of the input fields is resonant with the core transition (i.e. $\omega_1=\omega_0$), $\omega_1 \sim \omega_2 >> \omega_{ex}$, $n=3.5*10^{28}$ m^{-3}, $r_a=0.1$ nm, $\mathrm{sinc}^2(\delta k L_{int}/2)=0.8$, $L=\alpha^{-1}$ and $|E_1^A|^2=|E_1^B|^2=10^{20}$ V^2/m^2. The choice of the latter value relies upon the consideration that the power series reported in Eq. 1 does not necessarily converge for arbitrarily large values of |E|. In particular, when |E| approaches the atomic field strength ($E_{at} \sim e/(4\pi\varepsilon_0 a_0^2) \sim 5*10^{11}$ V/m; being a_0 is the Bohr radius) the non-linear response of materials is very different and Eq. 1 loses its validity.[5] Again, in the x-ray regime the efficiency of the FWM process significantly drops down, even for equal conditions in terms of phase matching factor and input field strength. This points out how the XUV coherent FEL pulses provided by FERMI are likely the more suited ones to make the first step in bringing coherent wave-mixing spectroscopy beyond the optical range. However, we have to stress that these estimates were done for a particular experiment based on the FEL two-colour emission developed of FERMI and sketched in Fig. 5d; other FWM processes in which both pump and probe pulses are tuned to core resonances may

have substantially larger $|\chi^{(3)}|$ values, even in the x-ray range.[14-17]

We finally recall that the ω_{ex} range exploitable in the experiment proposed in Fig. 5d is limited to below 1 eV (for ω's ~ 100 eV) by the the bandwidth of the FEL amplifier. This limits the range of detectable excitations to vibrational modes or low-energy electronic excitations, similarly to optical CRS, still with the option of atomic selectivity. However, the forthcoming development of novel multi-colour emission schemes can substantially enhance the potentiality of wave-mixing experiments that would be carried out at FERMI. In particular we mention an alternative approach (presently under testing) to generate a single FEL pulse that contains two photon frequencies, corresponding to the N^{th} and M^{th} harmonics of the seed laser. In this case values of $\Delta\omega=\omega_{ex}=(N-M)\omega_{UV}$ can be exploited, with the straightforward option to set ω_{ex} either by changing ω_{UV} and/or N and M.

5 Conclusions

We exploited the novel two-color seeded FEL emission scheme developed at the FERMI facility to carry out the first two-color FEL-pump/FEL-probe experiment. Data allowed us to determine the optical response of XUV photoexcited Ti close to the $M_{2/3}$-edge as a function of the excitation fluence on an ultrafast timescale. As a result, 0.5 ps after the action of the exciting (pump) pulse we observed the insurgence of an absorptionless behavior on increasing the excitation level of the sample, already reported in literature for much shorter (< 15 fs) timescales. The persistence of such a 'FEL-induced transparency' at times much longer than the characteristic core-hole recombination time can be interpreted as an indication that the highly ionized state induced by the pump partially survives when the electronic and ionic subsystems are thermalized (or during their thermalization). Furthermore, we also observed a FEL-induced dispersionless behavior, which develops with fluence paralleling the absorptionless one. This trend can be cast in the framework of a FEL-induced shift of the absorption edge, since we found a quantitative (though poorly accurate) agreement between the fluence evolution of both absorption and dispersion coefficients and the dependencies of such quantities on the probing photon frequency in the unexcited sample. We also stress that the measuring scheme discussed here allows for the determination of the time-evolution of the dielectric function in FEL-excited samples.

The discussed experiment demonstrated the reliability of the two-colour operation mode developed at FERMI and, though it did not directly exploited the coherence properties of the seeded FEL source, it represents a milestone in our efforts towards bringing the most advanced optical methods into the realm of XUV/soft x-rays. We hereby discussed on the possibility to exploit the coherence of such a two-colour FEL source to perform non-linear wave-mixing experiments at the EIS-TIMER beamline, a used-dedicated instrument devoted to the development of XUV/soft x-rays wave-mixing experiments. These coherent methods are nowadays limited to the optical domain, also in light of the lack of bright, ultrafast (possibly multi-colour) sources of coherent XUV/x-ray radiation. Such a lacking can be definitely filled by seeded FELs, which may also provide the unique option of a fully controlled multi-pulse/multi-colour FEL emission.

Acknowledgements

Authors acknowledge the support from the European Research Council through the grant 202804-TIMER, the Italian Ministry of University and Research through the grants FIRB-RBAP045JF2 and FIRB-RBAP06AWK3 and the regional government of Friuli Venezia Giulia through the grant Nanotox 0060 -2009. Authors gratefully thank all members of the FERMI Commissioning Team for their invaluable assistance in the preparation of the experiment and during the measurements.

References

[a] *Elettra-Sincrotrone Trieste S.C.p.A., S.S. 14 km 163,5 in AREA Science Park, I-34149, Basovizza, Trieste, Italy; Tel: +39 040 375 8202; E-mail: filippo.bencivenga@elettra.eu*
[b] *Elettra-Sincrotrone Trieste S.C.p.A., S.S. 14 km 163,5 in AREA Science Park, I-34149, Basovizza, Trieste, Italy; Tel: +39 040 375 8093; E-mail: claudio.masciovecchio@elettra.eu*

‡ For sake of simplicity we hereafter drop the symbol ħ and indicate the frequencies in energy units.
‡‡ Such a quite large value was found during this particular experiment; focal spots down of ~100 μm^2 are routinely achieved.

1 M. Cammarata *et al.*, *Nature Methods*, 2008, **5**, 881-886.
2 C. Bressler *et al.,* 2009, *Science,* **323,** 489-492.
3 G. Vankó *et al.,* 2010, *Angew. Chem. Int. Edn Engl.,* **49,** 5910-5912.
4 P. A. Frenken, A. E. Hill, C. W. Peters and G. Weinreich, *Phys. Rev. Lett.*, 1971, **7**, 118-119.
5 R. W. Boyd, *Nonlinear Optics* (Elsevier, Oxford, 2008).
6 P. D. Maker and R. W. Terhune, *Phys. Rev.*, 1965, **137**, A801-A818.
7 N. Bloembergen, *Recent Progress in Four-Wave Mixing Spectroscopy*, in Laser Spectroscopy IV, edited by H. Walther and K. W. Rothe, (Springer, Berlin, 1979).
8 L. Dhar, J. A. Rogers and K. A. Nelson, *Chem. Rev.*, 1994, **94**, 157-193.
9 E. T. J. Nibbering., D. A. Wiersma and K. Duppen, *Phys. Rev. Lett.*, 1991, **66**, 2464-2467.
10 S. Mukamel, *Principles of Nonlinear Optical Spectroscopy* (Oxford University, New York, 1995).
11 M. Terazima, K. Okamoto and N. Hirota, *J. Phys. Chem.*, 1993, **97**, 5188-5192.
12 G. Dadusc *et al., Proc. Natl Acad. Sci. USA*, 2001, **98**, 6110-6115.
13 D. Avisar and D. J. Tannor, *Phys. Rev. Lett.*, 2011, **106**, 170405.
14 S. Tanaka *et al., Phys. Rev. A*, 2001, **63**, 063405.
15 S. Tanaka and S. Mukamel *J. Chem. Phys.*, 2002, **116**, 1877-1891.
16 S. Tanaka and S. Mukamel *Phys. Rev. Lett.*, 2002, **89**, 043001.
17 O. Berman and S. Mukamel, *Phys. Rev. B*, 2004, *69*, 155104.
18 L. Gallmann, C. Cirelli and U. Keller, *Annu. Rev. Phys. Chem.*, 2012, **63**, 447-469.
19 T. E. Glover *et al*., *Nature*, 2012, **488**, 603-608.
20 A. A. Lutman *et al*., *Phys. Rev. Lett.*, 2013, **110**, 134801.
21 T. Hara *et al.*, *Nature Commun.*, 2013, **4**, 2919.
22 E. Allaria *et al., Nature Photon.*, 2012, **6**, 699-704.
23 E. Allaria *et al., Nature Photon.*, 2013, *7*, 913-918.
24 E. Allaria *et al., New J. Phys.*, 2012, **14**, 113009.
25 E. Allaria *et al., Nature Commun.*, 2013, **4**, 2476.
26 G. Gregori, S. H. Glenzer, W. Rozmus, R. W. Lee and O. L. Landen, *Phys. Rev. E*, 2003, **67**, 026412.
27 O. Gahl *et al.*, *Nature Photon.*, 2008, **2**, 165-169.
28 B. B. Pollock et al., *Rev. Sci. Instrum.*, 2012, **83**, 10E348.
29 E. Principi *et al.*, *Phys. Rev. Lett.*, 2012, **109**, 025005.
30 F. Bencivenga *et al.*, *Sci. Reports* (accepted).
31 R. W. Lee *et al.*, *J. Opt. Soc. Am. B*, 2003, **20**, 770-778.
32 R. J. Taylor, *The Stars: Their Structure and Evolution* (Cambridge University Press, Cambridge, 1994).

33 S. X. Hu, B. Militzer, N. N. Goncharov and S. Skupsky, *Phys. Rev. Lett.*, 2010, **104**, 235003.
34 B. Nagler *at al.*, *Nature Phys.*, 2009, **5**, 693-696.
35 G. Zimmerman and R. More, J. Quant. Spectrosc. Radiat. Transfer, 1980, **23**, 517.
36 S.-K. Son, H. N. Chapman and R. Santra, *Phys. Rev. Lett.*, 2011, **107**, 218102.
37 O. Ciricosta *et al.*, *Phys. Rev. Lett.*, 2012, **109**, 065002.
38 J. Gaudin *et al.*, *Phys. Rev. B*, 2013, **88**, 060101(R).
39 N. Medvedev *et al.*, *New J. Phys.*, 2013, **15**, 015016.
40 H. P. Freund and P. G. O'Shea, *Phys. Rev. Lett.*, 2000, **84**, 2861–2864.
41 M. Zangrando *et al.*, *Rev. Sci. Instrum.*, 2009, **80**, 113110.
42 E. Allaria *et al.*, *New J. Phys.*, 2010, **12**, 075002.
43 M. B. Danailov *et al.*, optics express (accepted).
44 G. De Ninno *et al.*, *Phys. Rev. Lett.*, 2013, **110**, 064801.
45 E. Pedersoli *et al.*, *Rev. Sci. Instrum.*, 2011, **82**, 04371.
46 F. Capotondi *et al.*, *Rev. Sci. Instrum.*, 2013, **85**, 051301.
47 L. Raimondi *et al.*, *Nucl. Instr. and Meth. A*, 2013, **710**, 131-138.
48 Fermi Commissioning Team, private communication.
49 D. Ratner *et al.*, *Phys. Rev. ST Accel. Beams*, 2012, **15**, 030702.
50 Centre for X-Ray Optics, database freely available at: http://henke.lbl.gov/optical_constants/.
51 M. Ohno and G. A. van Riessen, *J. Electron. Spectrosc.*, 2003, **128**, 1-31.
52 J. A. Giordmaine, *Phys. Rev. Lett.*, 1962, **8**, 19-20.
53 N. Bloembergen, *J. Opt. Soc. Am.*, 1980, **70**, 1429-1436.
54 F. Bencivenga *et al.*, *Proc. SPIE*, 2013, **8778**, 877807.
55 F. Bencivenga *et al.*, *New J. Phys.*, 2013, **15**, 123023.
56 F. Bencivenga and C. Masciovecchio, *Nucl. Instr. and Meth. A*, 2009, **606**, 785-789.
57 L. Misoguti *et al*., *Phys. Rev. A*, 2005, **72**, 063803.
58 K. Tamasaku, K. Sawada, E. Nishibori and T. Ishikawa, *Nature Phys.*, 2011, **7**, 705-708.
59 F. Bencivenga, *Nuovo Cimento C* (accepted).